

## Numerical study of island effects on Rayleigh waves

*J. P. Narayan*

Department of Earthquake Engineering, Indian Institute of Technology Roorkee

*Received 11 April 2005, in final form 25 September 2005*

To improve our understanding of Rayleigh wave generation and propagation in oceans, the effects of the presence of an island on the Rayleigh wave features are simulated. The analysis of results reveals Rayleigh wave generation in ocean near the island. In the water column, a decrease of amplitude in the vertical component and an increase of amplitude in the radial component of Rayleigh wave with depth are observed. The path of particle motion is elliptical clockwise, vertically polarised at the surface and horizontally polarised at the base of the water column. An increase of Rayleigh wave amplitude with island-slope ( $20^\circ - 60^\circ$ ) is obtained, in contrast to the decrease of Rayleigh wave amplitude with increase of slope of basin-edge in the basin. The effect of island-slope is greater in the vertical component, as compared to the radial one. Responses of different submersed islands (0 – 75 m below water surface) reveal decrease of amplitude of island-induced Rayleigh waves with depth. The obtained results help us to understand the characteristics and the generation of Rayleigh waves near islands.

*Keywords:* Island effects, Rayleigh wave generation and propagation in oceans.

### 1. Introduction

Effects of surface topography on the seismic wave propagation have received increasing interest recently due to day-by-day growth of population of structures on elevated topographies (Bard, 1982; Geli et al., 1988; Sánchez-Sesma and Campillo, 1991; 1993; Pedersen et al., 1994a). Certainly, in the past, there were numerous cases of recorded motion and the observed damage, pointing towards a topography-induced amplification (Celebi, 1987; 1991). Pedersen et al. (1994b) studied the effects of ridge topography on ground motion characteristics using recorded data across the Sourpi ridge, Central Greece and Mont Saint Eynard ridge in the French Alps. Narayan and Rao (2003) and Narayan (2003) reported a generation of surface waves near the top of the ridge. In this paper, the role of an island on the Rayleigh wave generation and its propagation is presented. Recordings near the island during earthquakes are not available; therefore, comparison with observed data was not possible.

Takenaka and Kennett (1996) developed 2.5-D time domain elastodynamic wave equation for plane wave incidence. Narayan (2001) reported good correlation of 3-D and 2.5-D amplitude behaviour and radiation patterns with each other in the  $xz$ -plane. 2.5-D modelling was used for the study of island effects on the generation of Rayleigh waves and their characteristics. The configuration for a 2.5-D wave simulation is achieved when medium properties vary only in two dimensions and source-receiver paths are confined in the same plane. The seismic responses of the models for different island-slope ( $20^\circ - 60^\circ$ ) and submersed islands up to depths of 75 m were computed.

## 2. Numerical simulations

Seismic responses of island models were computed using an algorithm based on second order parsimonious finite difference staggered grid approximation of a 2.5-D elastodynamic wave equation (Luo and Schuster, 1990; Ohminato and Chouet, 1997; Takenaka and Kennett, 1996). Double-couple shear dislocation point source based on moment tensor source formulation was implemented into the computational grid (Pitarka, 1999; Narayan, 2001). Both the absorbing boundary and Sponge boundary conditions were implemented on the model edges to avoid edge reflections (Clayton and Engquist, 1980; Israeli and Orszag, 1981). Vacuum formulation ( $V_P$ ,  $V_S$  and  $\rho \rightarrow 0$ ) was adopted in the region above the free surface.

During the model discretization, positive  $x$ -coordinate was pointing in north direction and positive  $z$ -coordinate was pointing vertically downward. Figure 1 shows the north-south cross section of the island model having a slope of  $45^\circ$ . For simplicity, the surface of island and water were taken at the same level. Distances were measured with respect to the centre of the island. The P- and

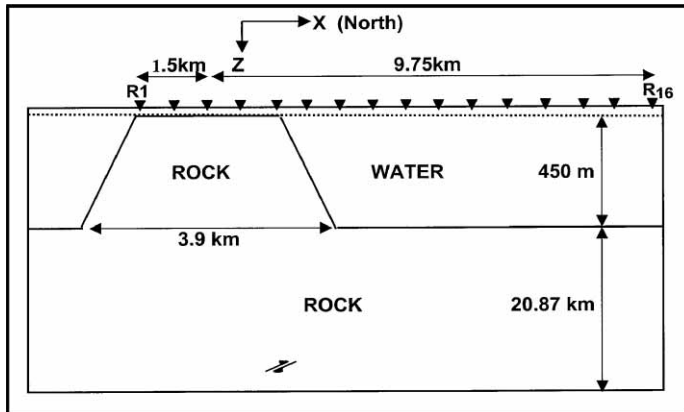


**Figure 1.** Vertically exaggerated island model (Note: two close parallel arrows show the double-couple point source).

S-waves velocities and densities were taken as 1458 m/s, 0.0 m/s and 1.02 g/cc in the water and 5196.2 m/s, 3000 m/s and 2.7 g/cc in the rock. Variable grid size was used in the descritization of the island model (14.0 km × 21.32 km). The horizontal dimension of the grids was 25 m and the vertical dimension of the grids was 25 m up to 1.1 km of depth and 150 m thereafter. The width of top of island was 3.0 km in all the cases. Time step was taken as 0.0025 s.

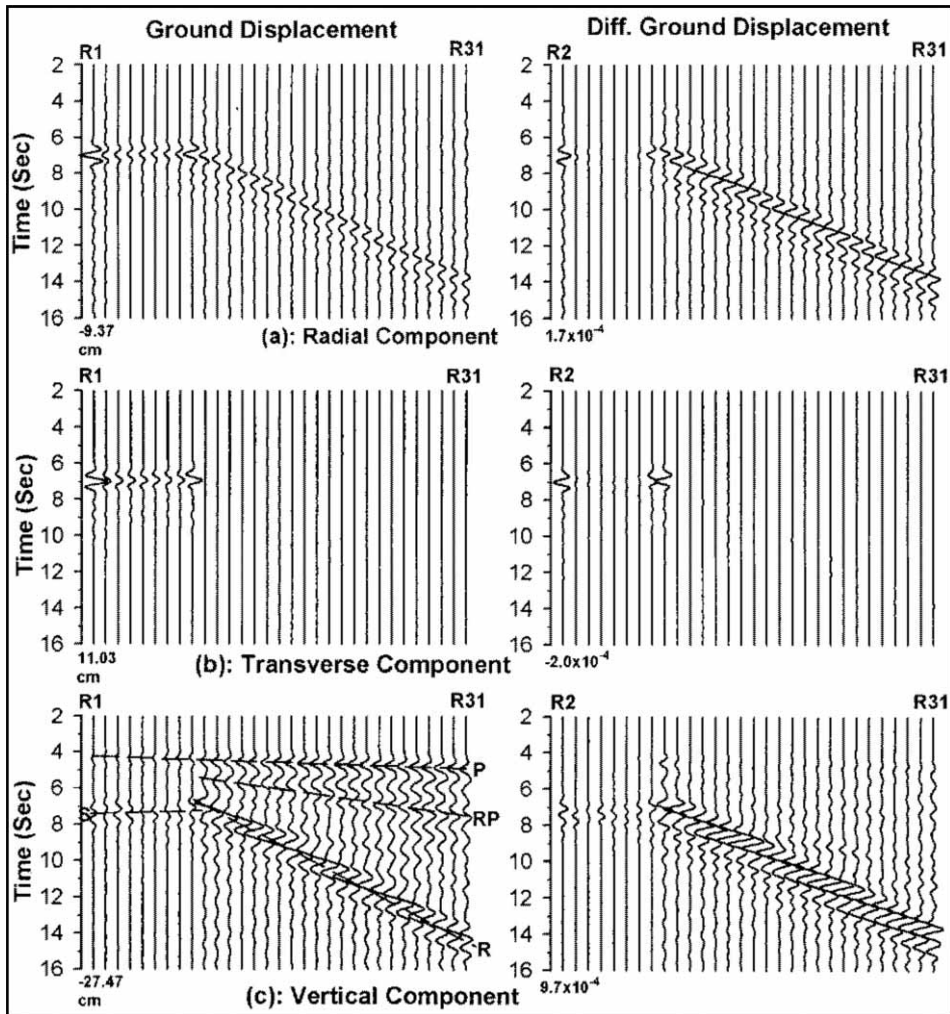


**Figure 2.** Radial, transverse and vertical components of ground displacement and differential ground displacement. The notations P, S, RP and R in plot c (left side) illustrate P-wave, S-wave, reflected P-wave from ocean bottom and Rayleigh wave, respectively. The notations used to show the identified seismic phases is also applicable for other plots of this figure (Note: Normalization factor for vertical component is ten times larger than that of horizontal component).

### 3. Analysis of simulation results

Seismic response of an island model with  $45^\circ$  slope was simulated using source (dip =  $90^\circ$ , rake =  $15^\circ$  and strike =  $30^\circ$ ) at a depth of 16.82 km and at an offset of 1.5 km from centre of the island, towards north. A Ricker wavelet with dominant frequency 1.0 Hz was used as the source excitation function. Different components of ground displacement were computed at 31 equidistant receiver points (375 m apart, from 1.5 km south to 9.75 km north of centre of the island).

The different components of ground displacement and the differential ground displacements  $\frac{\partial u}{\partial x}$ ,  $\frac{\partial v}{\partial x}$  and  $\frac{\partial w}{\partial x}$  are shown in figure 2 ( $u$ ,  $v$  and  $w$  are components of particle displacement in X, Y and Z-directions, respectively). The horizontal strains (differential ground motions), along the north–south direction were computed by simply dividing the difference of ground displacements at two adjacent receiver points by the distance between them.

Figure 2 shows an extra prominent seismic phase in the radial and vertical components of ground displacement with much lesser apparent velocity as compared to the body waves. In the differential ground motion, the vertically

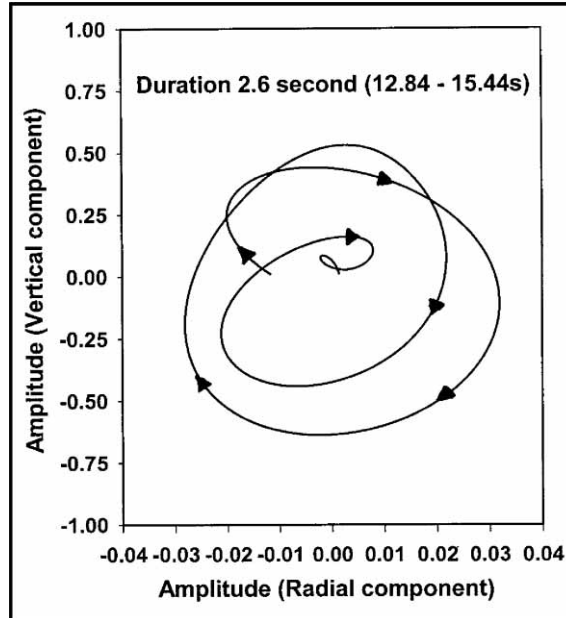


**Figure 3.** The path of particle motion at the water surface during the propagation of Rayleigh wave in a time window (12.84 – 15.44 s) and at an epicentral distance of 7.5 km towards north. The ground displacement in the radial and vertical components at different moments is plotted on X- and Y- axis, respectively.

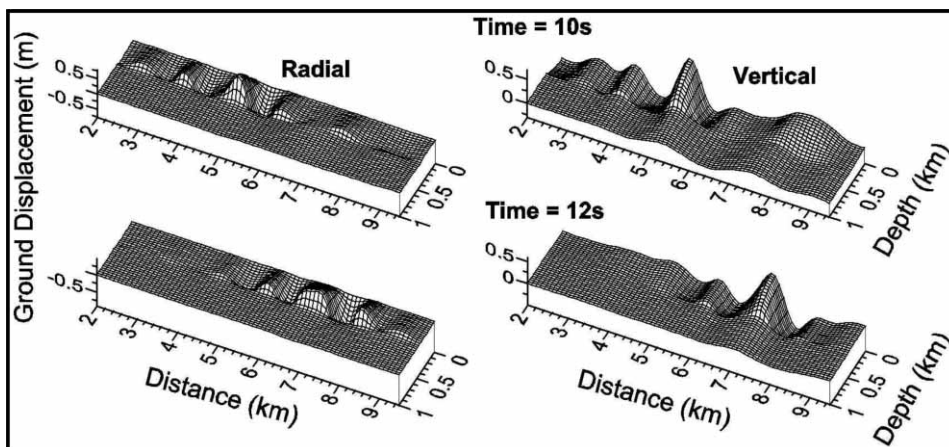


**Figure 4.** Snapshots of radial and vertical components of ground displacement in a vertical rectangular plane ( $7.5 \text{ km} \times 1.0 \text{ km}$ ) at 2.0 km north of island centre.

propagating body waves and reverberations are more or less eliminated and only the spatial derivatives of the horizontally travelling waves are present. These observations reveal that the horizontally travelling waves are Rayleigh waves. Rayleigh waves are caused by both the incident SV- and P-waves, but the amplitudes of Rayleigh wave caused by the P-wave is negligible as compared with the amplitude of Rayleigh wave caused by the S-wave (see differential ground displacement associated with radial component). The estimated Rayleigh wave group velocity is around 1170 m/s, somewhat lesser than the P-wave velocity in water for this particular model parameter. The particle displacement at the ocean surface in the radial and vertical components at different moments between a time window 12.84 – 15.44 s were used to draw the path of the particle motion (Fig. 3). Figure 3 clearly depicts that the path of particle motion during Rayleigh wave propagation is clockwise. The amplitudes of Rayleigh waves are about 4 – 5 times greater than that of SV-waves recorded on the top of the island.

Snapshots at times 10 s and 12 s in a rectangular region ( $7.5 \times 1.0 \text{ km}$ ) situated 2.0 km north of centre of island from surface to 1.0 km depth were computed (Fig. 4). Snapshots clearly indicate propagation of Rayleigh waves in the water and their amplitude variation with depth. The amplitude of Rayleigh wave in the vertical component is decreasing towards the bottom of the ocean but it is increasing in the radial component. The particle displacements (snapshots at times 10 s and 12 s) at distances of 5.0 km and 7.0 km were also used to study the Rayleigh wave amplitude variation with depth (Fig. 5). Figure 5 depicts the amplitude decay with depth in the vertical component and its increase in the radial component up to the base of the water column, with a sudden drop at the interface.

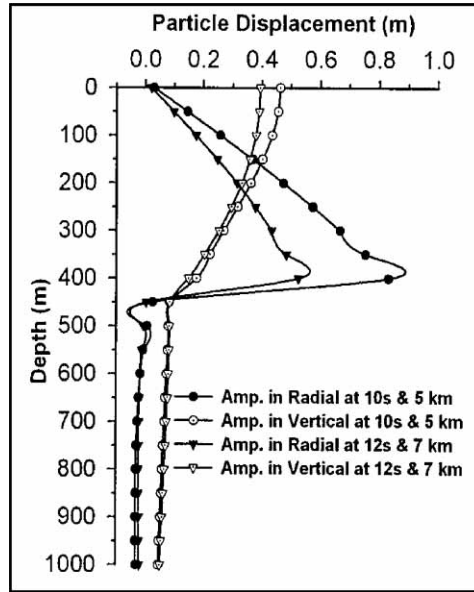


Figure 5. Rayleigh wave amplitude variation with depth at two locations.

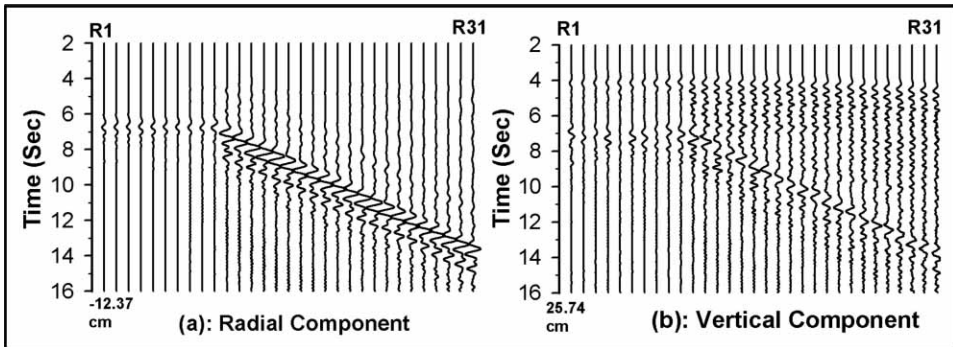
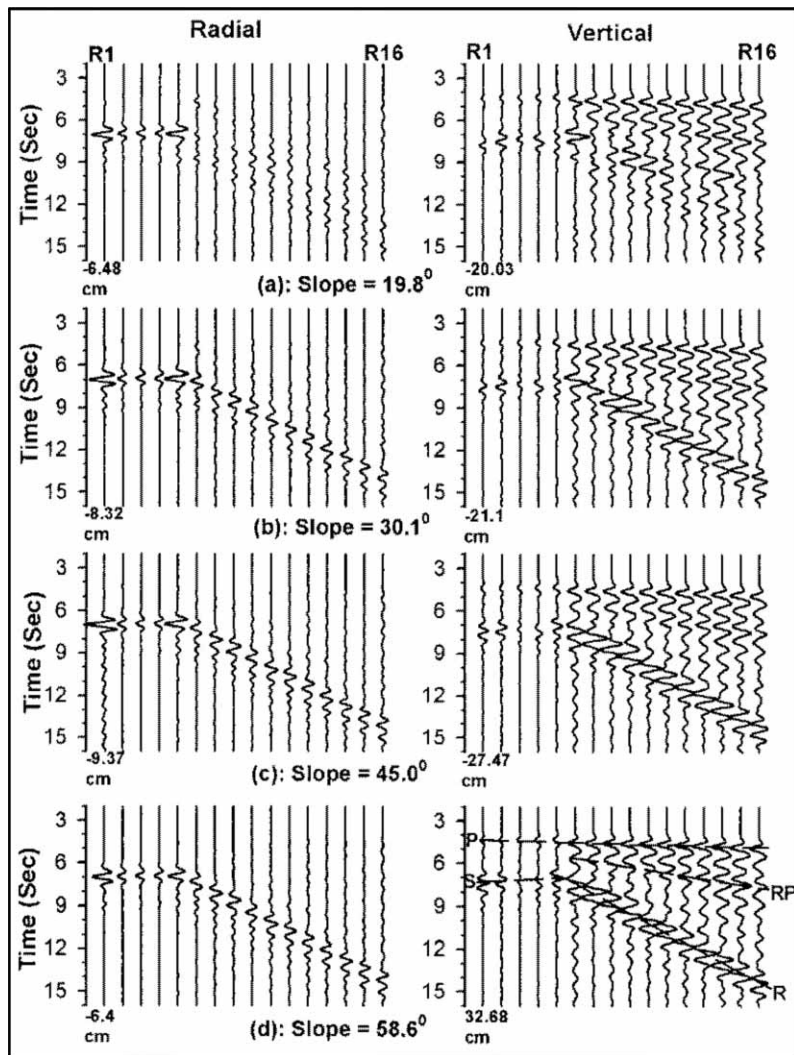


Figure 6. Radial and vertical components of ground displacement recorded at a depth of 400 m with the same source and receiver configuration as in figure 2. (Note: the criteria followed to show/identify the different seismic phases are also same as in figure 2.

For further confirmation of decrease of Rayleigh wave amplitudes in the vertical component and increase in the radial component with depth, seismic responses were computed at a depth of 400 m using the same model parameters, source and the receiver configuration. Figure 6 shows very large Rayleigh wave amplitudes in the Radial component as compared with the vertical component, as was predicted in figures 4 and 5.

3.1. Effects of island-slope

The radial and vertical components of responses of island models with different slopes ( $19.8^\circ$ ,  $30.1^\circ$ ,  $45.0^\circ$  and  $58.6^\circ$ ), computed at 16 equidistant (750 m apart) receiver points, are shown in figure 7. The analysis of this figure reveals



**Figure 7.** Radial and vertical components of ground displacement for different island slopes. The notations P, S, RP and R in plot 'd' (right side) illustrate P-wave, S-wave, reflected P-wave from ocean bottom and Rayleigh wave, respectively. The notations used to show the identified seismic phases are also applicable for other plots of this figure (Note: Normalization factor for vertical component is ten times larger than that of radial component)

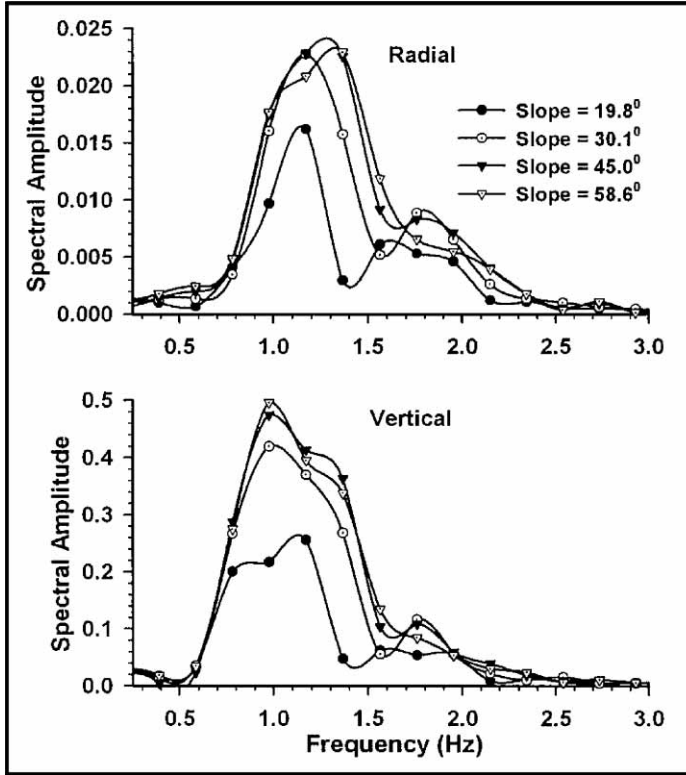


**Figure 8.** Fourier spectra of recorded ground displacement at receiver R15 (7.5 km north of epicentre) in radial and vertical components corresponding to Rayleigh wave arrival for different island-slope.

that the amplitudes of the Rayleigh waves are increasing with the increase of slope in both the components of ground motion. This finding is totally opposite to that obtained in the case of a basin, where Rayleigh wave amplitude decreases with the increase of the slope of the basin-edge (Bard, 1980 a & b; Narayan, 2005). For spectral analysis, data in a time window (12 s – 16 s) corresponding to the arrival of Rayleigh waves at receiver R15 was Fourier transformed into frequency domain.

The spectral amplitudes in the radial and vertical components for different slopes are shown in figure 8. There is an increase of spectral amplitudes with the slope increase in both components. A strong increase of spectral amplitude for island slope from  $19.8^\circ$  to  $30.1^\circ$  is observed. Dominant frequencies are between 1.2 – 1.4 Hz in the radial component and between 1.0 – 1.2 Hz in the vertical component. Further, dominant frequency is shifting towards higher values in the radial component and towards lower values in the vertical component with island slope. I conclude that an increase of the

slope of the island causes an increase of spectral amplitude of generated Rayleigh waves. This inferred effect seems to be greater in the vertical component as compared to the radial component.

### 3.2. Effects of a submerged island

Figure 9 shows only vertical component of ground displacement for different water column thickness covering the island top (00 m, 25 m, 50 m and 75 m). Results show that Rayleigh waves are generated in all the considered cases but their amplitudes are decreasing with increase of thickness of water column above the submersed island. The amplitude of Rayleigh waves in the responses of submersed island was found to be greater than the amplitude of SV-waves on the top of the island.

The Fourier spectra of signal recorded at receiver R15 in a time window of 4 s (12 s – 16 s) in the vertical component are shown in figure 10, for different thickness of water column above the submersed island. A decrease of spectral amplitudes with increase of thickness of water column at the top of the submersed island can be seen. There is strong drop ( $\approx$  two times) of Rayleigh wave spectral amplitudes in responses of submersed island at different depths as compared with the response of island. It may be concluded that submersed

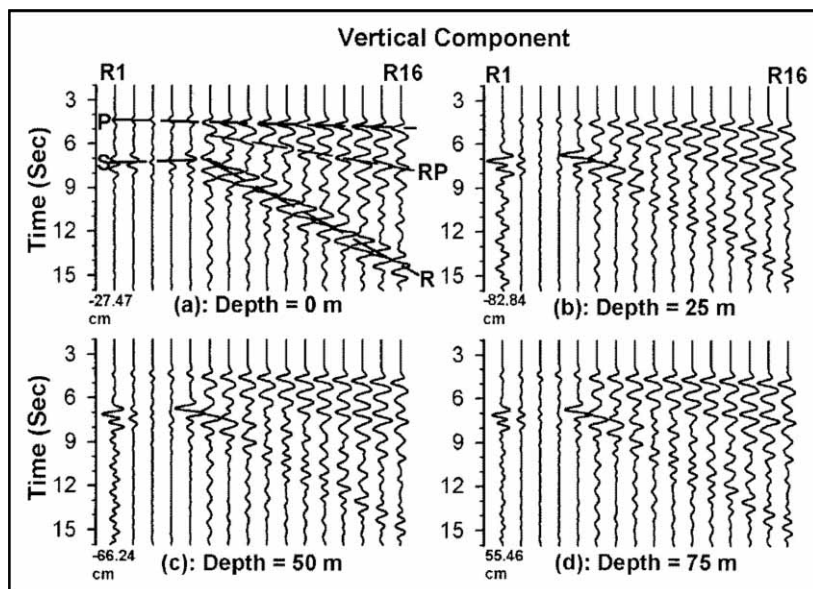


**Figure 9.** Vertical component of ground displacement for submersed island at different depths. The notations P, S, RP and R in plot 'a' (left side) illustrate P-wave, S-wave, reflected P-wave from ocean bottom and Rayleigh wave, respectively. The notations used to show the identified seismic phases are also applicable for other plots of this figure.

island also causes generation of Rayleigh waves, and Rayleigh wave amplitudes decrease with increase of thickness of water column at the top of the submersed island.

#### 4. Conclusions

An algorithm developed by Narayan (2001) was used in the 2.5-D simulations of the effects of island on the characteristics of the generated Rayleigh waves. The generation of Rayleigh waves near the island was confirmed on the basis of differential ground motion, large coherence among the recording stations, snapshots and estimated group velocity of later phases (around 1170 m/s). Recordings near an island during earthquakes is not available, therefore, author was unable to confirm the generation of Rayleigh waves near the island with the help of observed data. The decay of Rayleigh wave amplitudes with depth was observed in the vertical component. In contrast to this, an increase of Rayleigh wave amplitude in the radial component is obtained up to the base of the water column. The path of particle motion on the water surface is elliptical clockwise.

An increase of Rayleigh wave amplitudes with island slope was obtained in contrast to decrease of Rayleigh wave amplitude with slope of a basin edge, although in both the cases Rayleigh waves are developed in the low velocity medium (Bard, 1980 a & b; Narayan, 2005). The effect of island slope is greater in the vertical component as compared to the radial component. It is concluded on the basis of the analysis of responses of submersed island models at different depths that submersed island also causes Rayleigh wave generation but their amplitudes decrease with increase of thickness of water column at the top of the submersed island.

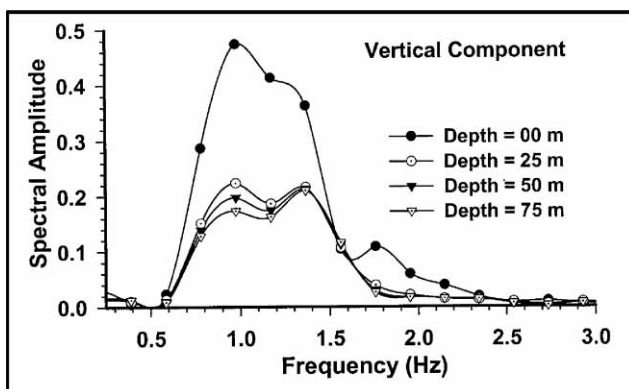


**Figure 10.** Fourier spectra of vertical component of ground displacement recorded at receiver R15 (7.5 km north of epicentre) corresponding to arrival of Rayleigh wave for different depths of submersed island.

*Acknowledgement* – Author is grateful to Department of Science and Technology (DST), New Delhi for financial support through grant No. DST-034-EQD. Author is also grateful to the two unknown reviewers for their valuable comments and suggestions, which have led to the great improvement in the original manuscript

## References

- Bard, P. Y. (1982): Diffracted waves and displacement fields over two-dimensional elevated topographies, *Geophys. J. Roy. Astr. S.*, **71**, 731–760.
- Bard, P. Y. and Bouchon, M. (1980a): The seismic response of sediment filled valleys, Part 1. The case of incident SH-waves, *B. Seismol. Soc. Am.*, **70**, 1263–1286.
- Bard, P. Y. and Bouchon, M. (1980b): The seismic response of sediment filled valleys, Part 2. The case of incident P and SV-waves, *B. Seismol. Soc. Am.*, **70**, 1921–1941.
- Celebi, M. (1987): Topographical and geological amplifications determined from strong-motion and aftershock records of the 3 March 1985 Chile earthquake, *B. Seismol. Soc. Am.*, **77**, 1147–1167.
- Celebi, M. (1991): Topographic and geological amplification: case studies and engineering implications, *Struct. Saf.*, **10**, 199–217.
- Clayton, R. W. and Engquist, B. (1980): Absorbing side boundary conditions for wave equation migration, *Geophysics*, **45**, 895–904.
- Geli, L., Bard, P. -Y. and Jullien, B. (1988): The effect of topography on earthquake ground motion: a review and new results, *B. Seismol. Soc. Am.*, **78**, 42–63.
- Israeli, M. and Orszag, S. A. (1981): Approximation of radiation boundary conditions, *J. Comput. Phys.*, **41**, 115–135.
- Luo, Y. and Schuster, G. (1990): Parsimonious staggered grid finite differencing of the wave equation, *Geophys. Res. Lett.*, **17**, 155–158.
- Narayan, J. P. (2001): Site specific strong ground motion prediction using 2.5-D modelling, *Geophys. J. Int.*, **146**, 269–281.
- Narayan, J. P. (2003): Simulation of ridge weathering effects on the ground motion characteristics, *J. Earthquake Eng.*, **7**, 447–461.
- Narayan, J. P. (2005): Study of basin-edge effects on the ground motion characteristics using 2.5D modelling, *Pure Appl. Geophys.*, **162**, 273–289.
- Narayan, J. P. and Rao, P. V. P. (2003): Two and half dimensional simulation of ridge effects on the ground motion characteristics, *Pure Appl. Geophys.*, **160**, 1557–1571.
- Ohminato, T. and Chouet, B. A. (1997): A free Rayleigh boundary condition for including 3D topography in the finite difference method, *B. Seismol. Soc. Am.*, **87**, 494–515.
- Pedersen, H., Sánchez-Sesma, F. J. and Campillo, M. (1994a): Three dimensional scattering by two-dimensional topographies, *B. Seismol. Soc. Am.*, **84**, 1169–1183.
- Pedersen, H., Hatzfeld, D., Campillo, M. and Bard, P. Y. (1994b): Ground motion amplitude across ridges, *B. Seismol. Soc. Am.*, **84**, 1786–1800.
- Pitarka, A. (1999): 3-D elastic finite difference modeling of seismic motion using staggered grids with non-uniform spacing, *B. Seismol. Soc. Am.*, **89**, 54–68.
- Sánchez-Sesma, F. J. and Campillo, M. (1991): Diffraction of P, SV and Rayleigh waves by topographical features: a boundary integral formulation, *B. Seismol. Soc. Am.*, **81**, 2234–2253.
- Sánchez-Sesma, F. J. and Campillo, M. (1993): Topographic effects for incident P, SV and Rayleigh waves, *Tectonophysics*, **218**, 113–125.
- Takenaka, H. and Kennett, B. L. N. (1996): A 2.5D time domain elastodynamic equation for plane wave incidence, *Geophys. J. Int.*, **125**, F5–F9.

## SAŽETAK

**Numeričko istraživanje efekta otoka na Rayleigheve valove***J. P. Narayan*

Kako bismo poboljšali razumijevanje nastanka i rasprostiranja Rayleighevih valova u oceanima simulirani su efekti otoka na obilježja Rayleigevih valova. Analizom rezultata pokazano je da se u oceanu u blizini otoka stvaraju Rayleighevi valovi. U vodenom stupcu se primjećuje smanjenje amplitude vertikalne komponente i povećanje amplitude radijalne komponente Rayleighevih valova s dubinom. Čestica se giba eliptično u smjeru gibanja kazaljke na satu, vertikalno je polarizirana na površini i horizontalno na dnu vodenog stupca. Zapaženo je povećanje amplitude Rayleighevog vala s nagibom otoka ( $20^{\circ}$ – $60^{\circ}$ ); nasuprot tome amplituda Rayleighevog vala u bazenu smanjuje se s povećanjem nagiba ruba bazena. Efekt nagiba otoka je veći u vertikalnoj komponenti nego u radijalnoj. Odziv različitih podvodnih otoka (0–75 m ispod površine vode) ukazuje na smanjenje amplitude s dubinom kod otokom induciranih Rayleighevih valova.

*Ključne riječi:* efekt otoka, nastanak i rasprostiranje Rayleighevih valova u oceanima

Author's address: J. P. Narayan, Department of Earthquake Engineering, Indian Institute of Technology Roorkee, Roorkee-247667, INDIA, e-mail: jaypnfeq@iitr.ernet.in.